Journal of Solid State Chemistry **161,** 266–273 (2001)
doi:10.1006/jssc.2001.9309, available online at http://www.idealibrary.com on IDEAL®

An Electron and X-Ray Diffraction Investigation of $Ni_{1+x}Te_2$ and $Ni_{1+x}Se_2$ *CdI_2/NiAs* Type Solid Solution Phases

L. Norén,*,[1] V. Ting,* R. L. Withers,* and G. Van Tendeloo†

*Research School of Chemistry, Australian National University, Canberra ACT 0200, Australia; and †EMAT, University of Antwerp (RUCA), Groenenborgerlaan 171, B-2020 Antwerp, Belgium

Received March 27, 2001; in revised form July 3, 2001; accepted July 12, 2001

The reported wide-range nonstoichiometric $Ni_{1+x}Te_2$, $0 \leq x \leq 0.83$, and $Ni_{1+x}Se_2$, $0.57 \leq x \leq 0.92$, *CdI_2/NiAs* structure type solid solution fields have been carefully reinvestigated via electron and X-ray powder diffraction to search for evidence of Ni/vacancy ordering and superstructure phases. In the case of telluride, evidence is thereby found for a Ni_3Te_4 superstructure phase attempting to condense out at $x \sim 0.5$ while, in the case of selenide, three quite distinct phases have been identified within the $Ni_{1+x}Se_2$ solid solution field. An intriguing characteristic honeycomb diffuse-intensity distribution has also been observed across the solid solution field in the case of the $Ni_{1+x}Te_2$ system. Its presence has been attributed to low frequency phonon modes along certain very specific directions of reciprocal space. © 2001 Academic Press

***Key Words:* *CdI_2/NiAs* solid solutions; phase analysis study; TEM; modulated structures.**

1. INTRODUCTION

Many initially reported to be homogeneous, wide-range nonstoichiometric solid solution fields, upon closer investigation, have been found to be modulated in one form or another—either in a long-range ordered modulated structure form giving rise to additional sharp satellite reflections in reciprocal space or in a locally ordered form leading to an often highly structured diffuse intensity distribution (1–5). A tendency toward ordering in solid solution systems is not surprising since the addition or removal of "guest" atoms from any "host" structure always changes, at least locally, coordination environments for both host and guest atoms leading to both local structural distortion and longer range strain interactions. The strength and range of the interactions between guest and host atoms presumably determines both the extent of ordering of the guest atoms at any one particular composition as well as the composition width of the solid solution itself.

If changes in occupancy can occur more-or-less at random, they can be adequately described via variable partial occupancies of the affected sites. The notion of the solid solution is then truly valid and no additional structured scattering is to be expected. On the other hand, if the strength of the interactions between host and guest atoms is rather strong, ordering and associated longer range structural relaxation is likely to take place giving rise (potentially) to new superstructure phases and weak additional structured scattering, which is usually difficult to detect via conventional X-ray diffraction techniques.

Electron diffraction, by contrast, is well suited to the detection of weak features of reciprocal space and is applied in this paper to search for evidence of ordering (and associated structural relaxation) in two reported wide-range nonstoichiometric solid solution fields (6), namely the $Ni_{1+x}Te_2$, $0 \leq x \leq 0.83$, (52–67 at% Te, Fig. 1a) and $Ni_{1+x}Se_2$, $0.57 \leq x \leq 0.92$ (see Fig. 1b), *CdI_2/NiAs* structure type solid solution fields. There has been much recent interest in the bonding and oxidation states of the constituent ions in late transition-metal chalcogenides of this type as a result of the tendency of the chalcogenide ions (particularly tellurium ions) to form multiple anionic bonds leading to anion polymeric networks (see (7–9) and references contained therein).

Transition-metal chalcogenides of this type are all based upon a common structural principle—a fully occupied, essentially hexagonal close packed (hcp) chalcogen array with the layer of octahedral interstices between successive hcp layers therein occupied by transition metal ions (see Fig. 2). These resultant transition-metal layers can be either fully or partially occupied. An almost universal occurrence in such systems is the alternation of fully occupied and partially occupied transition metal layers along the hcp stacking direction (10–12). The resultant average structure is then of "stuffed" CdI_2 type (space group symmetry $P\bar{3}m1$), whereas, if the alternate transition metal layers along the hcp stacking direction, **c**, are equally occupied, then the resultant average structure is of defect *NiAs* type (space

[1] To whom correspondence should be addressed. E-mail: lasse@rsc.anu.edu.au.

0022-4596/01 $35.00

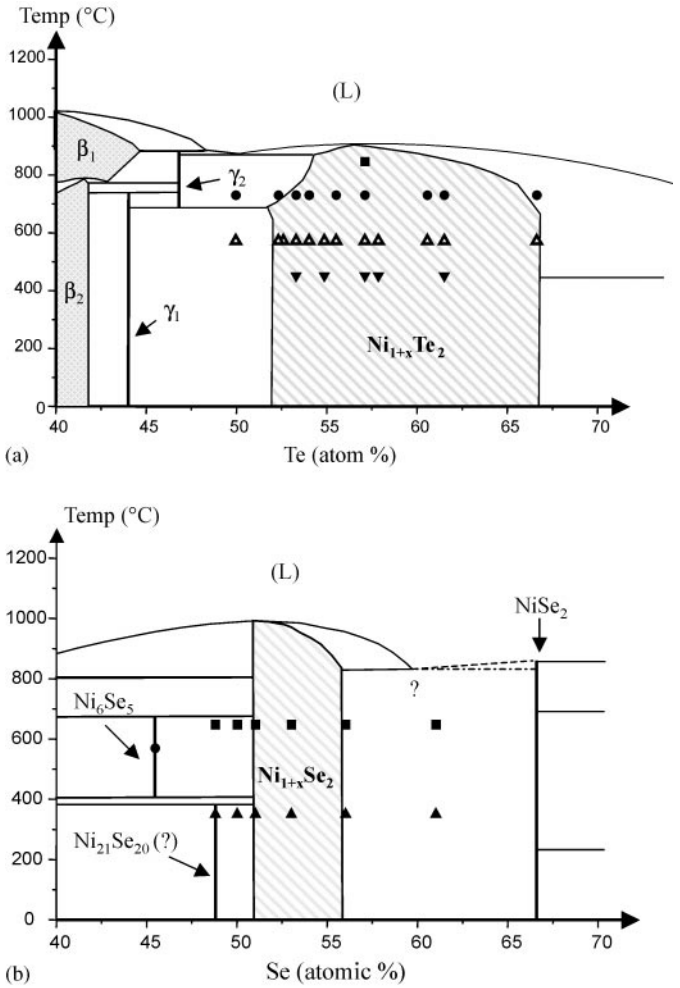

FIG. 1. The $CdI_2/NiAs$ and surrounding portions of the (a) Ni–Te and (b) Ni–Se binary phase diagrams as given in (6). The various compositions synthesized and annealing temperatures used are marked on the respective phase diagrams.

group symmetry $P6_3/mmc$). Any ordering of the vacancies both within and between these partially occupied transition-metal layers (and associated structural relaxation) should give rise to weak additional scattering accompanying the strong Bragg reflections of the underlying CdI_2 or $NiAs$ type average structure.

The $Ni_{1+x}Te_2$, $0 \leq x \leq 0.83$, solid solution studied in this paper has the widest reported composition range of any transition metal chalcogenide of this type and indeed was long considered to constitute the classic example of a continuous transition from the CdI_2 to the $NiAs$ structure type (13, 14). No evidence for superstructure phases arising from in-plane ordering of Ni atoms and vacancies (there is a layer stacking transition from CdI_2 to $NiAs$ type at $x \sim 0.6$) has ever been reported in this system (11, 12) by contrast with, for example, the $Cr_{1+x}Te_2$ system (6, 15), where Cr/vacancy ordered Cr_2Te_3, Cr_3Te_4; Cr_5Te_6 and Cr_7Te_8 superlattice phases are known to exist.

As a counterpoint to the $Ni_{1+x}Te_2$ solid solution, we decided to also study the $Ni_{1+x}Se_2$ solid solution in order to investigate the effect of the relative size of the chalcogen to transition metal (and, hence, indirectly the electronic bonding properties of the chalcogenide ion) upon phase behavior. The $Ni_{1+x}Se_2$, $0.55 \leq x \leq 0.92$, solid solution field, by contrast with the $Ni_{1+x}Te_2$ solid solution field, is reported to show a markedly smaller composition range (6). Nonetheless, Grønvold (16) and subsequently Jellinek (10) have reported evidence for the existence of three distinct phases, two of which are superstructure phases, within this composition range. These have never been confirmed, however, and are not reflected in the most recent phase diagrams for this system (6).

2. EXPERIMENTAL

2.1. Synthesis

The compounds were synthesized from the pure elements using a silica tube technique. The elements were made to react at 1273 K for an hour and then were rapidly quenched in water. No etching of the tubes was observed. The unbroken ampoule was then annealed at 1000 K for three to four days and then water quenched. The product was then ground, pressed into pellets, reannealed at various temperatures for times ranging from a few days up to a fortnight followed by water quenching. This was repeated several times in order to ensure a homogeneous compound. A range of annealing temperatures was used in order to investigate the effect of temperature upon ordering. Clearly, the annealing temperature should be high enough for Ni diffusion to take place but not so high that any tendency to ordering might be destroyed. The annealing temperatures used and the compositions chosen are given as points in the respective phase diagrams (see Fig. 1).

2.2. Characterization

The samples were examined by X-ray powder diffraction using a Guinier–Hägg camera with monochromatized Cu$K\alpha_1$ radiation. Silicon (NBS No.640, $a = 5.4310280$ Å, 22.5°C; (17)) was added as an internal standard for accurate determination of unit cell dimensions. Samples for electron microscopy were prepared by crushing and dispersing onto holey–carbon coated copper grids. These grids were then examined in a Philips EM430 Transmission Electron Microscope (TEM).

3. RESULTS AND DISCUSSION

3.1. X-Ray Powder Diffraction

3.1.1. The $Ni_{1+x}Te_2$ solid solution. The $CdI_2/NiAs$ parent unit cell dimensions of the $Ni_{1+x}Te_2$ samples quenched from 570°C are depicted in graph form in Figs. 3a–d. The

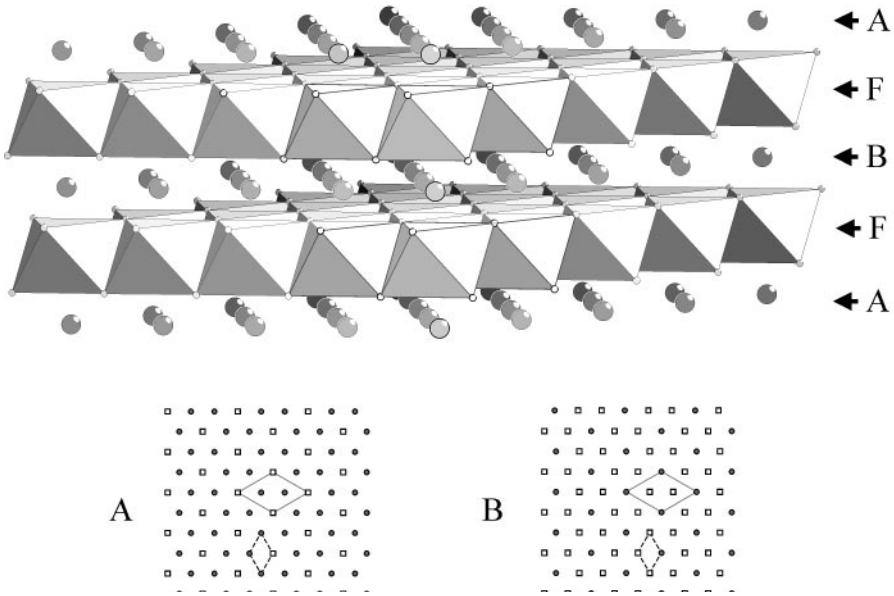

FIG. 2. A perspective view (close to ⟨110⟩) of the "stuffed" CdI_2 structure type. The chalcogen ions in the essentially hexagonal close packed (hcp) chalcogen array are represented by small balls. Octahedral layers within this essentially hcp array are occupied by transition metal ions. In the CdI_2 structure type, these transition metal layers are alternately fully occupied (represented by the octahedral layers and the symbol F) and partially occupied (represented by the large balls). Particular examples of partially occupied transition metal layers (labeled A and B) are shown in projection along **c** at the bottom of the figure. Occupied and vacant octahedral sites are here represented by filled circles and open squares, respectively.

solid solution range at this temperature was found to be slightly smaller than that reported in (6). $Ni_{1.82}Te_2$ was found to be a two-phase mixture, whereas $Ni_{1.80}Te_2$ was found to be single-phase solid solution. This places the nickel-rich boundary of the solid solution at $0.80 < x < 0.82$ at this temperature. The nickel poor region to the right of the thick dashed vertical line in Fig. 3 was found to be of the CdI_2 structure type while the area to the left of this

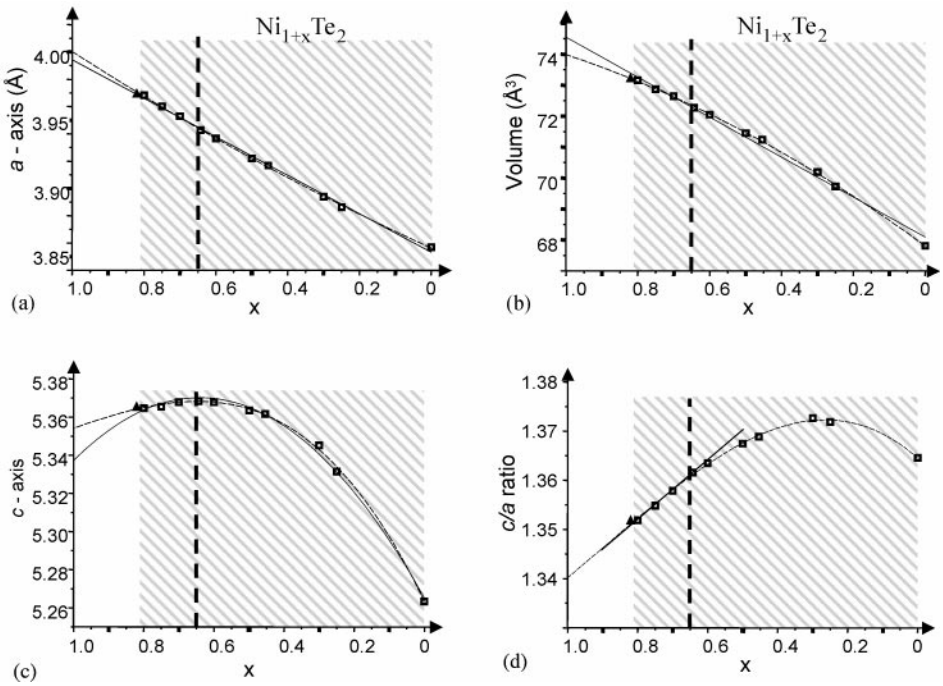

FIG. 3. The (a) a, (b) volume, (c) c, and (d) c/a ratio of the $CdI_2/NiAs$ parent unit cell of $Ni_{1+x}Te_2$ samples quenched from 570°C plotted as a function of composition (x). The gray hatched area represents the extent of the $CdI_2/NiAs$ solid solution field. Specimens to the right of the vertical dashed line were found to be of CdI_2 type while specimens to the left were found to be of $NiAs$ type.

line was found to be of *NiAs*-type, as judged by the appearance or otherwise of *NiAs*-forbidden reflections such as [0001]* (11, 12).

As is apparent from Fig. 3a, the *a*-axis of the unit cell increases essentially linearly with increasing nickel intercalation, the difference between a linear fit (solid line) and a second order polynomial fit (dashed line) being rather small. The volume of the unit cell (see Fig. 3b) as a function of Ni content is likewise also well described by a linear fit, although it appears that the volume increase is more rapid for the initial stages of intercalation (data points above the linear average) and less so toward the Ni-rich part of the solid solution range. By contrast, the *c*-axis as a function of Ni content clearly cannot be modeled by a linear fit (see Fig. 3c). A second-order polynomial (the solid line) gives a reasonable fit to most data points although there remain some problems in the Ni-rich region. A better fit is obtained via a third order polynomial (the dashed line). It is interesting to note that both these functions reach their maximum value at the composition for which a crossover from *NiAs* to CdI_2-structure type occurs, at $x \sim 0.65$. Finally, for the *c*/*a*-ratio (see Fig. 3d), there is an initial increase as Ni content increases until a maximum is reached at $x \sim 0.3$, beyond which the *c*/*a* ratio decreases gradually toward $x \approx 0.65$, after which it becomes more or less linear with increasing Ni content.

The fact that the *z* fractional coordinate of the Te ion in stoichiometric $NiTe_2$ (9, 12) is very close to $\frac{1}{4}$ (indeed it remains close to $\frac{1}{4}$ right across the whole solid solution field (12)) ensures that the thickness of the fully occupied Te–Ni_1–Te layer has essentially the same width as the (nickel vacant) Te–Ni_2–Te layer. In conjunction with the low *c*/*a* ratio ($\sim$1.365) and consequent short interlayer ("through layer" as well as "through gap") Te–Te distances (7, 9), it seems clear that interlayer Te–Te bonding is playing an important role in determining the thickness of the layers and hence the magnitude of the *c* axis.

The initial increase of the *c* axis when excess nickel is first introduced into $NiTe_2$ therefore seems most likely to be caused by the introduction of electrons into Te–Te antibonding states, leading to a weakening (and hence lengthening) of the interlayer Te–Te bonds and a consequent increase in magnitude of the *c* axis. As more nickel ions are introduced, this electronic effect upon the *c* axis appears to slowly fade until in the *NiAs*-type region of the solid solution we see a decrease of the *c* axis. This could be interpreted as a sign that Ni–Te bonding is becoming more and more important. It is also possible that this Ni–Te bonding is of more ionic character since the formal oxidation state of tellurium is now closer to its lowest value of -2.

3.1.2. The $Ni_{1+x}Se_2$ solid solution. Only synthesized samples within the $NiAs/CdI_2$ solid solution field (see Fig. 1b) were investigated in detail. Unlike for the $Ni_{1+x}Te_2$ solid solution field, it was immediately clear from the powder X-ray data that the underlying $NiAs/CdI_2$ unit cell does not change smoothly as composition is varied across the reported solid solution field. Monoclinic splitting of parent reflections, for example, were clearly observed for the $x = 0.57$ specimen but not for either the $x = 0.77$ or 0.92 specimens (see Table 1). Nonetheless, the parent unit cell volume systematically shrinks as Ni is removed and appears to obey Vegard's law.

TABLE 1
Unit Cell Parameters for $Ni_{1+x}Se_2$ (in Å) as a Function of Composition *x* (Samples Quenched from 370°C (see Fig. 1b))

x	*a*	*b*	*c*	*β*	*V*
0.92	3.6559(4)	*	5.3510(9)	90	61.937(18)
0.77	3.6344(6)	*	5.3213(11)	90	60.872(22)
0.57a	3.6359	*	5.2529	90.64	59.366
b	12.1460(10)	3.6360(5)	6.2175(7)	120.140(8)	237.46(5)
c	6.2174(8)	3.6357(5)	10.5058(12)	90.636(12)	237.47(5)

Note. The first line refers to the $NiAs/CdI_2$ parent cell or to a slightly distorted monoclinic variant thereof (a). The unit cells of the superstructures are refined in the standard *C*-centred settings (b) as well as in the settings used in Ref. (19) (c).

For the $x = 0.92$ specimen, a clean diffraction pattern was observed where all lines could be indexed with respect to a *NiAs* type parent structure. When *x* was lowered to 0.77, however, weak additional lines were observed which could not initially be indexed. Such behavior is strongly reminiscent of the recently reported $P'\bar{3}m1$ (ε, 0, 0; 0, ε, 0) 11 incommensurately modulated phase region in the $Co_{1+x}Se_2$ ($0.70 < x < 0.94$) system (18) (and indeed the X-ray powder pattern of $Ni_{1.77}Se_2$ was successfully indexed using the corresponding (3 + 2)-index notation giving a magnitude for ε of 0.450(5) (see the Electron Diffraction section below for more details on the indexation procedure).

The sample with the lowest nickel content ($x = 0.57$) showed clear monoclinic splitting of the parent reflections and additional superstructure reflections which could all be indexed using a monoclinic cell similar to that used for the Cr_3Se_4-type region of the Co–Se solid solution field (18, 19). The refined cell parameters are given in Table 1.

It is clear that the selenide exhibits a much stronger tendency for long-range ordering (of the Ni vacancies) than the telluride with at least three distinct phases being apparent from XRPD.

3.2. Electron Diffraction

3.2.1. The $Ni_{1+x}Te_2$ solid solution. The $Ni_{1+x}Te_2$ solid solution was investigated first. The initial specimens studied were $Ni_{1.45}Te_2$ (57.97% Te) and $Ni_{1.50}Te_2$ (57.14% Te) annealed at a range of different temperatures (see Fig. 1a) before rapid quenching. Two quite characteristic types of

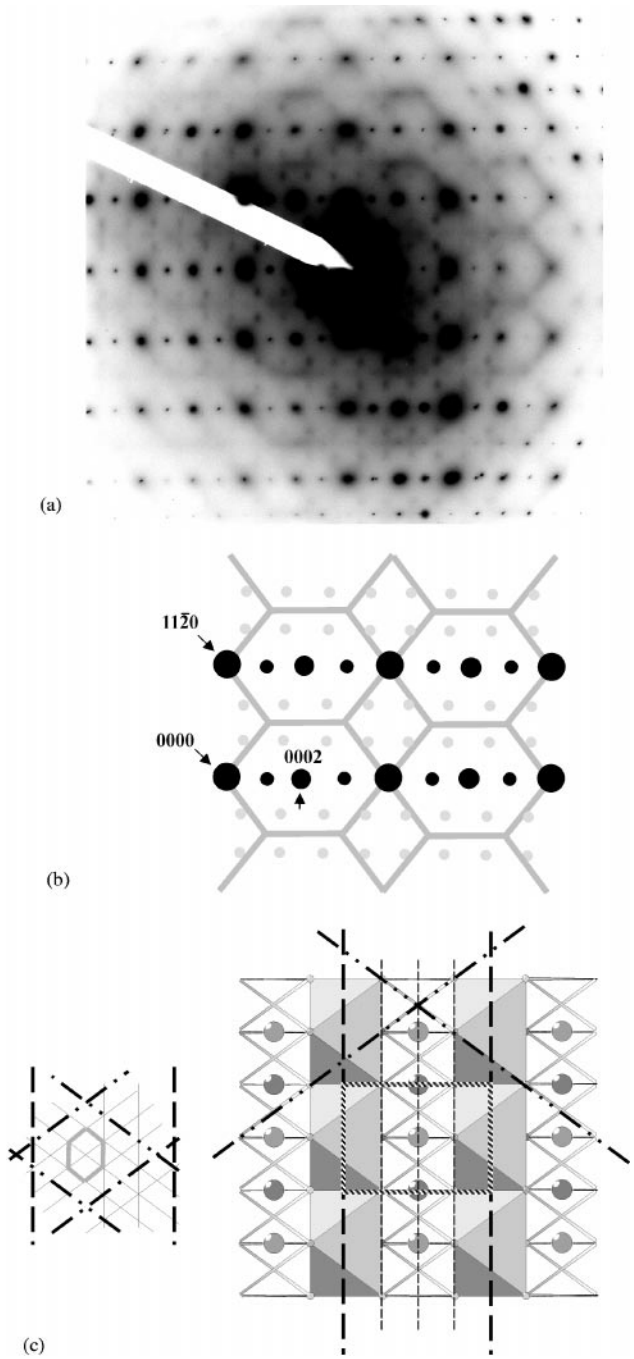

FIG. 4. (a) A typical close to $\langle \bar{1}10 \rangle$ zone axis EDP of $Ni_{1.45}Te_2$ (57.97% Te) annealed at 450°C for a week and (b) a schematic representation of the $\mathbf{G} \pm [\frac{1}{3}, \frac{1}{3}, \frac{-2}{3}, \frac{1}{2}]^*$ "satellite reflections" and honeycomb diffuse distribution observed in such close to $\langle \bar{1}10 \rangle$ zone axis EDP's. (c) The $\{11\bar{2}2\}$ and [0001] planes of real space (shown in projection by the dashed lines) orthogonal to the lines of diffuse streaking making up the honeycomb diffuse distribution in reciprocal space (cf. with Fig. 4b). The real space honeycomb network orthogonal (or dual) to the diffuse honeycomb network of reciprocal space is shown by the thick gray lines on the left-hand side of (c). The four $\{11\bar{2}2\}$ and [0001] type planes of atoms per parent $CdI_2/NiAs$ parent unit cell are shown by the thin solid lines again on the left-hand side of (c).

weak additional scattering, in addition to the strong Bragg reflections of the underlying $CdI_2/NiAs$ type parent structure, were always observed at orientations in the close vicinity of $\langle \bar{1}10 \rangle$ (see, for example, Fig. 4a which shows a typical close to $\langle \bar{1}10 \rangle$ zone axis electron diffraction pattern (EDP) of $Ni_{1.45}Te_2$ (57.97% Te) annealed at 450°C for a week).

The first type of weak additional scattering observed consisted of slightly diffuse "satellite reflections" centered on the $\mathbf{G} \pm [\frac{1}{3}, \frac{1}{3}, \frac{-2}{3}, \frac{1}{2}]^*_p$ regions of reciprocal space (see Figs. 4 and 5). (**G** here represents the set of strong Bragg reflections of the underlying CdI_2 type parent structure, and 4-index notation is used here and in what follows for reflections or reciprocal space features indexed with respect to the $NiAs/CdI_2$ type parent structure.) These satellite reflections only occur for compositions near $x \sim 0.5$ suggesting the existence of small domains or precipitates of a Ni/vacancy ordered Ni_3Te_4 superstructure phase attempting to "condense out" at this composition. Perhaps somewhat surprisingly, the temperature of annealing did not to all intents and purposes affect either the presence or sharpness of these satellite reflections. Figure 5, for example, shows a somewhat closer to $\langle \bar{1}10 \rangle$ zone axis EDP of $Ni_{1.50}Te_2$ (57.14% Te) annealed at 850°C for 48 h before rapid quenching. The $\mathbf{G} \pm [\frac{1}{3}, \frac{1}{3}, \frac{-2}{3}, \frac{1}{2}]^*$ satellite reflections are clearly still present suggesting that the Ni/vacancy ordering presumed responsible is already present even at quite high temperature. Prolonged annealing did not appreciably sharpen these satellite reflections.

Given that the presence of the satellite reflections is strongly dependent upon composition, the most plausible explanation for this Ni_3Te_4 "superstructure phase" is the Ni/vacancy ordered model shown in Fig. 2. The proposed

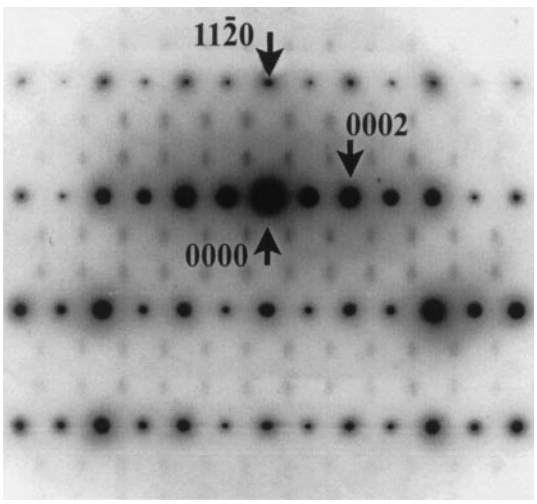

FIG. 5. A close to $\langle \bar{1}10 \rangle$ zone axis EDP of $Ni_{1.50}Te_2$ (57.14% Te) annealed at 850°C for 48 h before rapid quenching. Note the presence of the $\mathbf{G} \pm [\frac{1}{3}, \frac{1}{3}, \frac{-2}{3}, \frac{1}{2}]^*$ satellite reflections.

Ni layer stacking sequence is FAFBF etc., where F stands for the fully occupied Ni layers and A and B represent $\frac{2}{3}$ occupied and $\frac{1}{3}$ occupied Ni layers as shown in the bottom portion of Fig. 2, i.e., an alternation from a fully occupied Ni layer (F) firstly to a $\frac{2}{3}$ occupied layer A then back to an F layer followed by a $\frac{1}{3}$ occupied layer B and then back to the original F layer. Note that the basal plane unit cell of both the A and B layers is expanded by $\sqrt{3}$ relative to the underlying parent unit cell thus giving rise to the $[\frac{1}{3}, \frac{1}{3}, \frac{-2}{3}]$* basal plane component of $[\frac{1}{3}, \frac{1}{3}, \frac{-2}{3}, \frac{1}{2}]$* while the alternation from A to B and back of the partially occupied Ni layers explains the observed $\frac{1}{2}$ **c*** component of $[\frac{1}{3}, \frac{1}{3}, \frac{-2}{3}, \frac{1}{2}]$*. Such a model is entirely compatible with the observed diffraction evidence as well as the composition ($x \sim 0.5$) for which the superlattice reflections are observed.

Attempts to image the ordering by high-resolution electron microscopy along $\langle \bar{1}10 \rangle$ failed. Though the obtained images show the average structure perfectly, no ordering could be detected. In addition, EDP's retaken after imaging no longer showed the initially present satellite reflections. The nickel/vacancy ordering is clearly easily destroyed by electron beam irradiation.

The second characteristic and quite reproducible type of additional scattering observed takes the form of a highly structured, honeycomb-like diffuse intensity distribution involving reasonably sharp lines of diffuse intensity running along the $\langle 11\bar{2}2 \rangle$* and [0001]* directions of reciprocal space in close to $\langle \bar{1}10 \rangle$ zone axis EDP's (see, for example, Fig. 4a). (This diffuse distribution is, however, rather weak so that the exposure time used must be sufficient for it to be visible. The apparent absence of the diffuse distribution in Fig. 5, for example, arises from this cause.) Note that the $\mathbf{G} \pm [\frac{1}{3}, \frac{1}{3}, \frac{-2}{3}, \frac{1}{2}]$* satellite reflections described above, while close, do not fall onto this characteristic diffuse intensity distribution (see Fig. 4b).

The sharpness of these $\langle 11\bar{2}2 \rangle$* and [0001]* lines of diffuse intensity implies reasonably long range correlation (which could be Ni/vacancy occupational and/or displacive in character) within the orthogonal $\{11\bar{2}2\}$ and [0001] planes of real space (shown in projection by the corresponding dashed lines in Fig. 4c). The real space honeycomb network orthogonal (or dual) to the honeycomb network apparent in reciprocal space is shown by the thick grey lines on the left-hand side of Fig. 4c. Note the scale of this real space honeycomb network relative to the parent structure imposed by the diffraction evidence, e.g., the $\frac{1}{4}$ $\mathbf{c}_p$ repeat in real space corresponding to the 4 $\mathbf{c}_p^*$ repeat in reciprocal space, etc.

There are four $\{11\bar{2}2\}$ and [0001] type planes of atoms per parent *CdI*$_2$/*NiAs* parent unit cell (marked by the thin solid lines on the left-hand side of Fig. 4c). While each of these four planes could in principle scatter independently, the shape and scale of the observed honeycomb diffuse distribution (e.g., the effective "extinction condition" corresponding to the fact that the $\langle 11\bar{2}2 \rangle$* diffuse streaking runs essentially only through the $l = 4n$ (n an integer) parent reflections (see Figs 4a and 4b) requires all four such planes to scatter coherently in order to be understood (5, 20). Indeed it requires that the effective scattering power of each such plane (essentially the product of the average atomic scattering power multiplied by the displacement eigenvector (20) of the atoms in that plane) must be the same. The fact that the prime contribution to the observed diffuse distribution is displacive in character does not, however, per se preclude an occupational Ni/vacancy origin or stabilization for the displacive shifts.

One argument which suggests that the observed honeycomb diffuse distribution might well be of a pure displacive (or phonon) nature is its stability to electron beam irradiation. If Ni/vacancy ordering were required in order to stabilize the displacive shifts giving rise to the observed honeycomb diffuse distribution, then one might have expected the honeycomb diffuse distribution to be easily destroyed by the electron beam. If there is no Ni/vacancy occupational ordering underlying or inducing the atomic shifts primarily responsible for the observed diffuse distribution, then the displacive shifts must presumably correspond to very low frequency (virtually "soft"), thermally excited phonon modes. Why such phonon modes should be soft, i.e., sufficiently strongly excited to be visible at room temperature or why the reciprocal space distribution of such soft phonon modes should necessarily be so anisotropic in reciprocal space is far from clear.

The $\langle 11\bar{2}2 \rangle$* and [0001]* lines of diffuse intensity in Fig. 4(a) have a finite (although not large) "thickness" along the close to $\langle \bar{1}10 \rangle$ projection direction, which is apparent from EDP's taken tilted a few degrees away from the exact $\langle \bar{1}10 \rangle$ zone axis orientation. (The diffuse disappears altogether, however, if the orientation is too far from $\langle \bar{1}10 \rangle$.) Figure 6, for example, shows edp's of (a) $Ni_{1.25}Te_2$, (b) $Ni_{1.50}Te_2$, and (c) $Ni_{1.81}Te_2$ specimens taken tilted ~ 5–7° from the exact $\langle \bar{1}10 \rangle$ zone axis orientation while keeping the $\langle 11\bar{2}0 \rangle$* systematic row (running vertically) excited. Note that the same characteristic honeycomb-like diffuse intensity distribution is visible for each composition, i.e., virtually across the whole solid solution field.

Unlike for the satellite reflections, where their existence or otherwise was closely tied to composition, the existence and shape of the honeycomb diffuse distribution appears to be virtually independent of composition. Like the satellite reflections, however, the temperature of annealing makes very little difference to the presence or sharpness of this characteristic and quite reproducible diffuse distribution.

3.2.2. The $Ni_{1+x}Se_2$ "solid solution". The initial specimen investigated was $Ni_{1.57}Se_2$ (56.00% Se) annealed at two different temperatures (see Fig. 1b) before rapid quenching. In either case, satellite reflections of the form $\mathbf{G} \pm \frac{1}{2}\langle \bar{1}101 \rangle$*

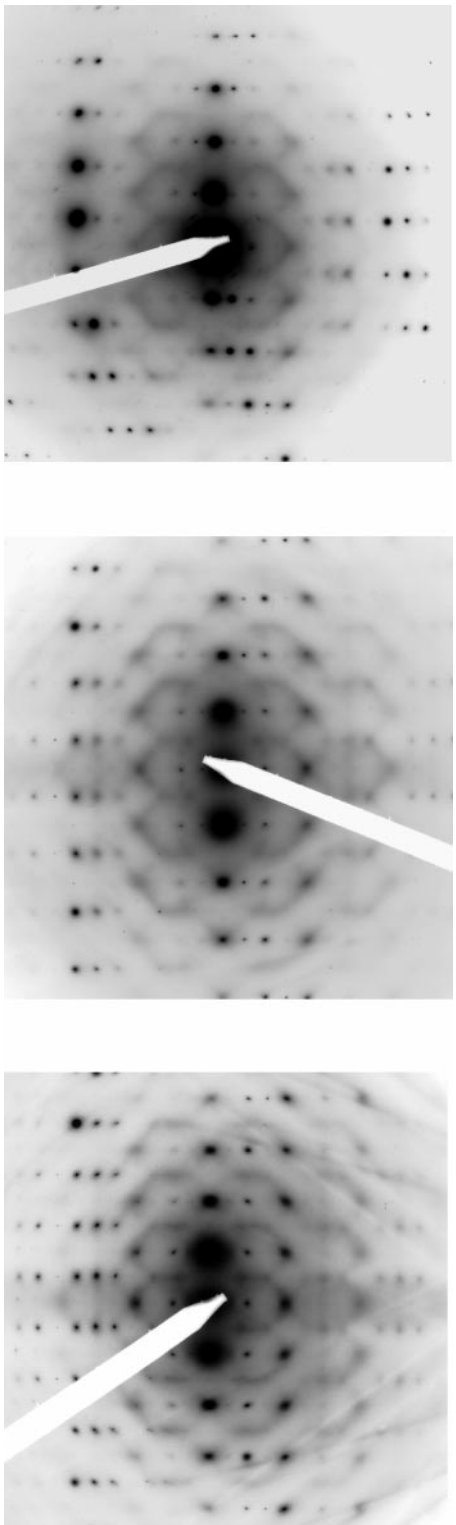

FIG. 6. EDP's of (a) $Ni_{1.25}Te_2$, (b) $Ni_{1.50}Te_2$, and (c) $Ni_{1.81}Te_2$ specimens taken tilted ~ 5–7° from the exact $\langle \bar{1}10 \rangle$ zone axis orientation while keeping the $\langle 11\bar{2}0 \rangle^*$ systematic row (running vertically) excited. Note that exactly the same characteristic honeycomb-like diffuse intensity distribution is visible for each composition, i.e., virtually across the whole solid solution field.

were clearly present in addition to the CdI_2 type parent structure Bragg reflections **G**. There are three potential "primary" modulation wave vectors of the form $\frac{1}{2}\langle \bar{1}101 \rangle^*$ (related by the threefold axis of the CdI_2 parent structure), i.e., $\frac{1}{2}\,[\bar{1}101]^*_p$, $\frac{1}{2}\,[0\bar{1}11]^*_p$ and $\frac{1}{2}\,[10\bar{1}1]^*_p$ (p for CdI_2 parent). In any one local region, however, only one such modulation wave vector of this type was ever found to exist, i.e., the additional satellite reflections were all, say, of the form $\mathbf{G} \pm \frac{1}{2}[\bar{1}101]^*_p$.

An I-centered, $\mathbf{a}_I = -\mathbf{a}_p + \mathbf{b}_p$, $\mathbf{b}_I = \mathbf{a}_p + \mathbf{b}_p$, $\mathbf{c}_I = -2\mathbf{c}_p$ lattice (corresponding reciprocal space unit cell vectors $\mathbf{a}^* = \frac{1}{2}\,[\bar{1}100]^*_p$, $\mathbf{b}^* = \frac{1}{2}\,[11\bar{2}0]^*_p$, $\mathbf{c}^* = \frac{1}{2}\,[0001]^*_p$) is thus required. This superstructure phase would thus appear to be isomorphous to the $I2/m$, $\mathbf{a} = -\mathbf{a}_p + \mathbf{b}_p$, $\mathbf{b} = \mathbf{a}_p + \mathbf{b}_p$, $\mathbf{c} = -2\mathbf{c}_p$, $Cr_{3\pm x}Se_4$ phase (19). (Note that the standard $C2/m$ setting of this space group corresponds to the unit cell choice $\mathbf{a}_C = -\mathbf{a}_I - \mathbf{c}_I = \mathbf{a}_p - \mathbf{b}_p + 2\mathbf{c}_p$, $\mathbf{b}_C = \mathbf{b}_I = \mathbf{a}_p + \mathbf{b}_p$, $\mathbf{c}_C = \mathbf{a}_I = -\mathbf{a}_p + \mathbf{b}_p$.) This is also consistent with the earlier results of Grønvold (16) who reported a monoclinic $\sqrt{3}\ a_p \times a_p \times 2c_p$ superstructure phase (although without giving a space group) for $x < 0.66$. Grønvold (16) reported a monoclinic angle of $\beta = 90.52^\circ$ for $x = 0.60$. This monoclinic splitting is also clearly apparent in the XRD patterns of our $x = 0.57$ sample (see Table 1).

The next specimen investigated was $Ni_{1.77}Se_2$ (53.00% Se) again annealed at two different temperatures (see Fig. 1b) before rapid quenching. Incommensurate satellite reflections of the form $\mathbf{G} \pm \sim\langle -0.45,\ +0.45,\ 0,\ \frac{1}{3}\rangle^*_p$ were present in both specimens as shown in the typical $\langle 110 \rangle$ selected area Electron Diffraction Pattern (EDP) of Fig. 7a. There are six (initially symmetry-equivalent) potential primary modulation wave vectors of $\langle -0.45,\ +0.45,\ 0,\ \frac{1}{3}\rangle^*_p$ type assuming $6/mmm$ Laue symmetry (appropriate if the average structure is of $P6_3/mmc$, $NiAs$ type). The average structure tertiary c glide is broken, however, which is clear from the presence of $[hh\bar{2}hl]^*_p$ reflections for which $l \neq$ even in the $\langle 110 \rangle_p$ zone axis EDP's of Fig. 7a as well as from the (essentially single domain) $\langle 110 \rangle_p$ zone axis EDP of Fig. 7b in which satellite reflections of the form $\mathrm{G} \pm \sim[-0.45,\ +0.45,\ 0,\ \frac{1}{3}]^*_p$ are present but not satellite reflections of the form $\mathbf{G} \pm \sim[-0.45,\ +0.45, 0,\ -\frac{1}{3}]^*_p$, i.e., the mirror plane perpendicular to the c axis is locally broken. The $\langle 110 \rangle_p$ EDP of Fig. 7a is thus from a twinned crystal region.

Do the three symmetry-related incommensurate primary modulation wave vectors ($\mathbf{q}'_1 = [-\varepsilon, \varepsilon, \frac{1}{3}]^*_p$, $\mathbf{q}'_2 = [\varepsilon, 0, \frac{1}{3}]^*_p$ and $\mathbf{q}'_3 = [0,\ -\varepsilon, \frac{1}{3}]^*_p$, $\varepsilon \sim 0.45$) simultaneously coexist in any one local region? The fact that the basal plane component of these incommensurate primary modulation wave vectors is irrational, whereas the c^*_p component is "locked in" to the rational value of $\frac{1}{3}$, exactly strongly suggests that they do. That $\mathbf{q}'_1 + \mathbf{q}'_2 + \mathbf{q}'_3 = c^*_p$ exactly regardless of the value of ε means that there is a corresponding Landau free energy term which "locks in" the component of the primary modulation wave vectors along the c^*_p reciprocal space

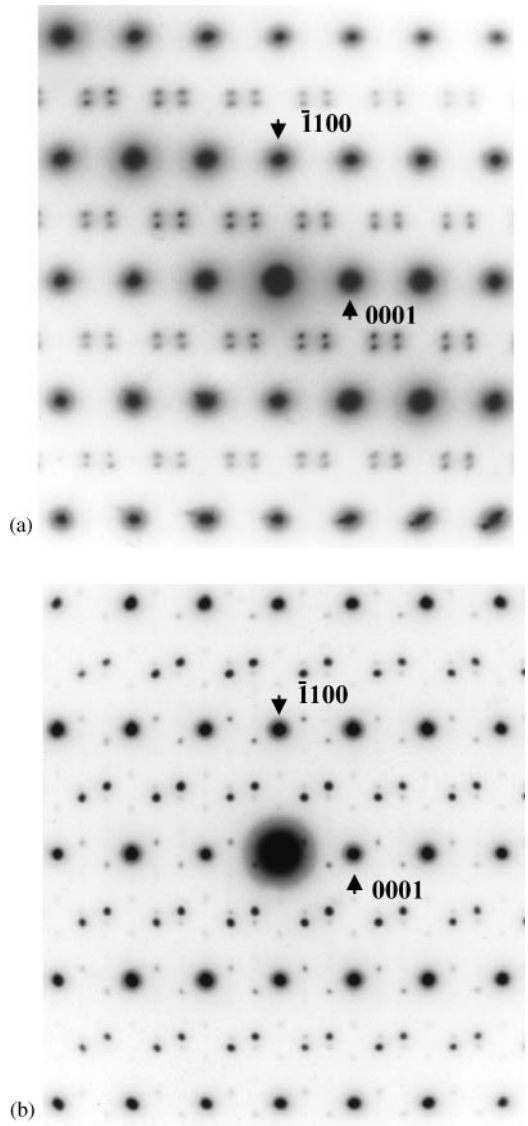

FIG. 7. The $\langle 110 \rangle$ zone axis EDP's of $Ni_{1.77}Se_2$ (typical of the (3 + 2)-dimensional incommensurately modulated phase). Note that satellite reflections of the form $\mathbf{G} \pm \sim[-0.45,\ +0.45,\ 0,\ \frac{1}{3}]^*_p$ are present in (b) but not satellite reflections of the form $\mathbf{G} \pm \sim[-0.45,\ +0.45,\ 0,\ -\frac{1}{3}]^*_p$, i.e., the mirror plane perpendicular to the *c* axis is locally broken. The $\langle 110 \rangle_p$ EDP of (a) is thus from a twinned crystal region.

direction without locking in the orthogonal basal plane components.

This phase is thus isomorphous to a (3 + 2)-dimensional incommensurately modulated phase recently discovered in the $Co_{2-x}Se_2$ system at a similar composition (18). The $\langle 110 \rangle$ zone axis EDP's of this phase are essentially identical to those shown in Fig. 7. Grønvold (16), by contrast, reported an orthorhombic $\sqrt{3}\ a_p \times 3a_p \times 3c_p$ superstructure phase ($\mathbf{a} = \mathbf{a}_p - \mathbf{b}_p$, $\mathbf{b} = 3(\mathbf{a}_p + \mathbf{b}_p)$, $\mathbf{c} = 3\mathbf{c}_p$; $\mathbf{a}^* = \frac{1}{2}\ [\bar{1}100]^*_p$ $\mathbf{b}^* = \frac{1}{6}\ [11\bar{2}0]^*_p$, $\mathbf{c}^* = \frac{1}{3}\ [0001]^*_p$) for $x = 0.26$. This is clearly not compatible with our observations.

The final specimens investigated were $Ni_{1.92}Se_2$ (51.00% Se) and $Ni_{2.00}Se_2$ (50% Se). In agreement with the previously reported phase diagram, the latter specimen was found to be two phase suggesting that it is not possible to make the ideal $Ni_{2.00}Se_2$ composition at this temperature. EDP's of the end-member $Ni_{1.92}Se_2$ (51.00% Se) specimen only showed *NiAs* type parent reflections in agreement with Grønvold (16).

4. CONCLUSIONS

The tendency for Ni/vacancy ordering is clearly very much weaker in the $Ni_{1+x}Te_2$ *CdI*$_2$/*NiAs* type solid solution field than in the corresponding $Ni_{1+x}Se_2$ solid solution field. This is reflected in the rather wider *CdI*$_2$/*NiAs* type solid solution field in the former case. Nonetheless clear evidence has been found for a Ni_3Te_4 superstructure phase attempting to condense out at $x \sim 0.5$ in the $Ni_{1+x}Te_2$ system. In the case of the selenide, three quite distinct phases have been identified within the $Ni_{1+x}Se_2$ solid solution field.

REFERENCES

1. S. Esmaeilzadeh, S. Lundgren, U. Halenius, and J. Grins, *J. Solid State Chem.* **156,** 168 (2001).
2. S. Lidin, *Acta Crystallogr. Sect. B* **54,** 97 (1998).
3. R. L. Withers, A.-K. Larsson, and S. Schmid, *J. Solid State Chem.* **149,** 218 (2000).
4. J. Billingham, P. S. Bell, and M. H. Lewis, *Acta Crystallogr. Sect. A* **28,** 602 (1972).
5. A.-K. Larsson, R. L. Withers, and L. Stenberg, *J. Solid State Chem.* **127,** 222 (1996).
6. T. B. Massalski (Ed.), "Binary Alloy Phase Diagrams." American Society for Metals, Metals Park, OH, 1986.
7. S. Jobic, R. Brec, and J. Rouxel, *J. Solid State Chem.* **96,** 169 (1992).
8. E. Canadell, S. Jobic, R. Brec, J. Rouxel, and M.-H. Whangbo, *J. Solid State Chem.* **99,** 189 (1992).
9. W. Bensch, W. Heid, M. Muhler, S. Jobic, R. Brec, and J. Rouxel, *J. Solid State Chem.* **121,** 87 (1996).
10. F. Jellinek, *in* "MTP International Review of Science, Inorganic Chemistry Series I," Vol. 5, pp. 339–396. Butterworths, London, 1972.
11. J. S. Anderson, *Proc. Indian Acad. Sci. Chem. Sci.* **93,** 861 (1984).
12. P. Coffin, A. J. Jacobson, and B. E. F. Fender, *J. Physics C* **7,** 2781 (1984).
13. J. Barstad, F. Grønvold, E. Røst, and E. Vestersjø, *Acta Chem. Scand.* **24,** 1036 (1970).
14. K. O. Klepp and K. L. Komarek, *Monatsh. Chem.* **103,** 934 (1972).
15. Y. Hinatsu and T. Tsuji, *J. Solid State Chem.* **154,** 356 (2000).
16. F. Grønvold, *Acta Chem. Scand.* **24,** 1036 (1970).
17. M. Hart, *J. Crystal Growth* **55,** 409 (1981).
18. L. Norén, R. L. Withers, F. J. García-García, and A.-K. Larsson, *Solid State Sci.*, in press.
19. T. Ohtani, R. Fujimoto, H. Yoshinaga, M. Nakahira, and Y. Ueda, *J. Solid State Chem.* **48,** 161 (1983).
20. F. Brink, R. L. Withers, and J. G. Thompson, *J. Solid State Chem.* **155,** 359 (2000).